

Analysing the fAPAR Dynamic Over Europe Using MODIS Data

Carmelo Cammalleri, Fabio Micale, Jürgen Vogt

European Commission, Joint Research Centre (JRC)

21027 Ispra (VA), Italy

e-mails: carmelo.cammalleri@jrc.ec.europa.eu; fabio.micale@jrc.ec.europa.eu; juergen.vogt@jrc.ec.europa.eu.

Abstract—This paper analyses the temporal dynamic of long-term fraction of Absorbed Photosynthetically Active Radiation (fAPAR) time series over Europe as derived from a 15 years dataset of satellite images collected between 2001 and 2015 from the Moderate-Resolution Imaging Spectroradiometer (MODIS) sensor onboard of Terra satellite. A fitting of piecewise logistic functions of time was performed for each cell in order to account for the multi-cycle dynamic of fAPAR. Most of the cells within the domain area showed a single peak cycle, even if a non-negligible fraction of the domain (about 15%) showed two distinct peaks in the yearly cycle. The results of the logistic function fittings allow identifying the key transition dates between increasing/decreasing trends in fAPAR, constituting a starting point for a more detailed analysis of drought effects on ecosystems.

Keywords- *fAPAR; vegetation cycle; EDO; MODIS.*

I. INTRODUCTION

The understanding of the phenological cycle of land ecosystems is a key element in the analysis of the feedbacks between climate and Earth's biosphere. The fraction of Absorbed Photosynthetically Active Radiation (fAPAR) has been widely identified as a suitable proxy of the greenness and health status of vegetation, thanks to its central role in both plant primary productivity and carbon dioxide absorption. The Global Climate Observing System (GCOS) recognized fAPAR as one of the 50 climate variables essential to characterize the climate of the Earth [1].

The spatiotemporal variability of fAPAR can be derived from space by means of the inverse solution of the radiation transfer through the canopy space. Several remote sensing based fAPAR products are currently available, including the ones from the Advanced Very High Resolution Radiometer (AVHRR), the Moderate-Resolution Imaging Spectroradiometer (MODIS) and the PROBA-V; particularly, the MODIS standard product MOD15A2 is characterized by a relatively long time series (starting in 2000) and a near real time update.

The observed sensitivity of fAPAR to vegetation stress has suggested its use in drought monitoring [2] [3]; an example is the role of fAPAR anomalies in the Combined Drought Indicator (CDI) developed for agricultural drought monitoring in the European Drought Observatory (EDO) [4] [5].

Even if the simple fAPAR anomalies have proven to be reliable for drought detection [6], the fAPAR response to drought may vary as a function of the timing and

phenological phase (i.e., early stage, late growth) [7], this latter characterized by a temporal variability influenced by climate change [8]. Generally, it seems valuable to quantify the capability to automatically identify the phenological stage at which a certain fAPAR anomaly occurs.

Several methodologies have been proposed in the past to capture the timing of key phenological phases in remote sensing fAPAR time series, including fixed thresholds [9], moving averages [10], lagged moving average [11], Fast Fourier and Harmonic Analysis [12], and fitting of smooth functions [13] [14], as well as to evaluate the impact of climate and used datasets on key transition dates [8] [15].

In this paper, we test the use of a series of piecewise logistic functions to fit a time series of fAPAR images collected by the MODIS-Terra sensor over Europe in the period 2001-2015. Advantage of logistic function is the capability to reproduce the succession of relatively constant low and high values linked by transition periods, as observed in most fAPAR records.

Goal of the study is to identify the suitability of the methodology to detect the key transition dates for a future integration of this approach in an operational drought monitoring system like EDO. In Section II, the processing of satellite data and the mathematical background of the fitting procedure are described, in Section III the main results of the fitting, including the detected number of peaks and the key transition dates, are detailed, and, finally, in Section IV a summary of the results is reported, as well as some key conclusions of the study are illustrated.

II. MATERIALS AND METHODS

In this Section, the pre-processing of the remotely sensed data, as well as the procedure to derive the key transition dates, are described in details.

A. Satellite fAPAR data

Physically based fAPAR retrieval algorithms commonly perform a combined estimation of fAPAR and Leaf Area Index (LAI). The standard MODIS Terra LAI/fAPAR product (MOD15A2, Collection 5) is used in this study; this product is available globally as 8-day composites at 1-km spatial resolution on a Sinusoidal grid. Data are provided in spatial tiles of about $1,200 \times 1,200 \text{ km}^2$ [16].

The estimation procedure retrieves LAI and fAPAR from the remotely-observed and atmospherically corrected Bidirectional Reflectance Distribution Function (BRDF) recorded by MODIS in 7 spectral bands by solving an

inverse problem. A numerical inversion of the three-dimensional radiation transfer process through the canopy system is solved by splitting it into two separate sub-problems: i) the radiation field in the canopy calculated for a black surface, and ii) the radiation field in the same medium (with the black surface) generated by anisotropic sources located at the canopy bottom [17].

Once information on the canopy structure is available, the solution to these problems is obtainable. Hence, a Look-Up-Table (LUT) approach is adopted by subdividing the vegetated land into eight-biome classes: grasses and cereal crops, shrubs, broadleaf crops, savanna, deciduous broadleaf forests, evergreen broadleaf forests, deciduous needle forests, evergreen needle forests.

The MOD15A2 product is generated daily and successively aggregated to 8-day composites by using a maximum composite method; quality assessment (QA) flags are included in the 8-day composition, and a back-up algorithm is triggered for low quality pixels to estimate LAI and fAPAR from vegetation indices. Data from MODIS-Terra are available from April 2000 to nowadays.

For the period 2001-2015, we downloaded the MOD15A2 tiles covering Europe (from 17 to 21 horizontal and from 02 to 05 vertical). A series of post-processing procedures was applied to the 8-day fAPAR tiles in order to obtain dekadal maps (3 maps per month, corresponding to the days: 1-10, 11-20 and 21-end of the month) over the European domain. First of all, the tiles were mosaicked and reprojected in the common lat/lon regular grid at 0.01 degree resolution. Hence, low quality data were masked out according to the QA flag and fAPAR estimates for each dekad were obtained by means of an exponential smoothing (with smoothing parameter equal to 0.5) of the raw data [18]. The exponential smoothing allows removing likely outlier (i.e., cloud contaminated values) without compromising a near-real time delivery of the newly upcoming data.

A long-term average fAPAR dataset is reconstructed by simply averaging the 15 values available for each dekad, obtaining an estimate of the mean fAPAR dynamic for each cell in the domain.

B. Fitting procedure

Ecological studies have shown clear temporal patterns in fAPAR time series, in which periods of relatively constant low and high values are linked by transition (smooth increasing/decreasing) periods; these patterns can be relatively well represented by means of a sequence of logistic functions [19].

This approach was introduced by [13] for an automatic application on MODIS Enhanced Vegetation Index (EVI) images, with the aims of modelling a single growth/senescence cycle from remotely sensed data. These authors suggest subdividing the full period into segments of sustained increasing/decreasing values, each of which can be fitted by the function:

$$y(t) = \frac{c}{1 + \exp(a + bt)} + d \quad (1)$$

where t is time in dekad, d is the minimum fAPAR value observed in the segment, $c+d$ is the maximum fAPAR value, a and b are the fitting parameters obtained from a least squares regression of the reduced variable $Y = \ln[c/(fAPAR-d)] - 1$ vs. t .

The key transition dates are identified from the fitted values $y(t)$ as the local extrema in the rate of change in curvature (derivative of the angle of the unit tangent of the curve along the unit length of the curve), K' :

$$K' = b^3 cz \left\{ \frac{3z(1-z)(1+z)^3 [2(1+z)^3 + b^2 c^2 z]}{[(1+z)^4 + (bcz)^2]^{5/2}} - \frac{(1+z)^2 (1+2z-5z^2)}{[(1+z)^4 + (bcz)^2]^{3/2}} \right\} \quad (2)$$

where $z = \exp(a + bt)$. Equation (2) presents three extrema (see Figure 1), the first is the onset of increasing fAPAR (circle), the second is the inflection point (cross) and the third is the onset of the maximum fAPAR values (square). In case of a segment with decreasing fAPAR values, the first and the last extrema represent the end of the period with maximum values and the end of the decreasing, respectively.

The fitting procedure is preceded by a segmentation phase, in which the single decreasing/increasing periods are identified. In this preliminary step a 5-value moving window average is performed on the fAPAR data, and the independent segments are identified in correspondence of the changes from positive to negative slope [19].

III. RESULTS

As described in Section II.B, a preliminary analysis of the fAPAR dekadal average data was performed in order to detect the number of segments necessary for an accurate fitting of the fAPAR annual cycle. As depicted in Figure 2, this analysis shows how most of the domain is characterized by a single cycle with a distinct peak (2 segments), even if a significant fraction of the domain (around 15%) presents 2 different peaks (4 segments) within the annual cycle.

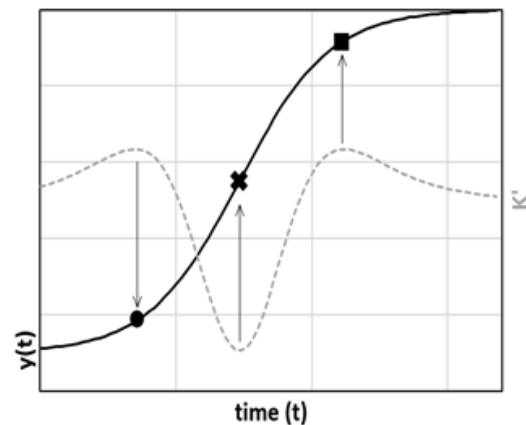


Figure 1. A schematic representation of the fitting procedure for a single segment (redrawn from [13]).

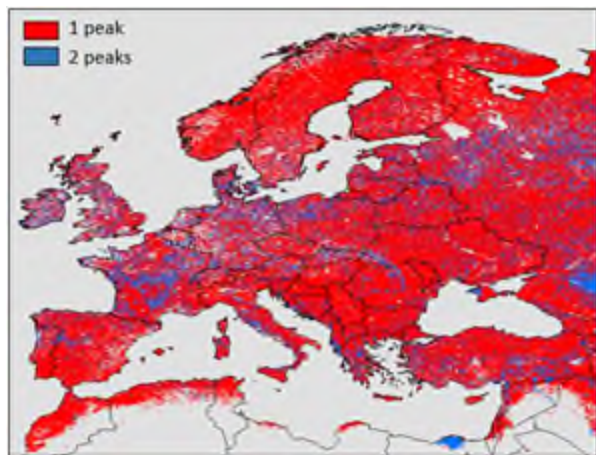


Figure 2. Spatial distribution of the cells with a single peak (in red) or with two peaks (in blue).

Distinct areas with two peaks in the processed window are the Nile (even if outside Europe) and Volga deltas, as well as some mountainous forests (i.e., Carpathian, Central Chain in Spain). It is worth to point out that a small fraction of the domain (around 8%) has no clear cycle according to our detection method, and an even smaller fraction ($< 2\%$) has more than 2 peaks (likely due to noisy time series); both areas were removed from the successive analyses.

The average fAPAR data were fitted according to a series of piecewise logistic functions, which number has been identified in the previous phase. For each cell, the key transition dates were evaluated, and two maps have been created as reported in Figure 3: a) starting Day Of the Year (DOY) of the increasing phase, and b) ending DOY of the decreasing phase.

The maps in Figure 3 show a quite large range of variability for both start and end dates, with distinct spatial patterns; in details, start date (Figure 3a) is early in the year (DOY 90) for Central Europe, is in the middle of the year for North Europe and quite late (DOY > 280) for the Mediterranean areas. Similarly, end date map (Figure 3b) shows a distinct North/South gradient, with end date just before summer for the Mediterranean countries, close to the end of the year for central Europe and around DOY 280-300 for North Europe. The North/South gradient observed in both transition dates is in general agreement with the expected phenological cycles for such regions.

The frequency distribution of the data in Figure 3a shows that the mode of the distribution is around DOY 130 ± 60 , even if a secondary small peaks can be observed at DOY = 290 (Mediterranean area). In contrast, the frequency distribution of the data in Figure 3b shows two overlapping bells around DOY 280 ± 15 and 330 ± 30 , corresponding to North-Central and South-Central Europe (respectively), and a quite small third peak at DOY 210 (Mediterranean areas).

The resulting length of the period between the start of the increasing and the end of the decreasing fAPAR (not shown) has a single peak distribution centered on DOY = 230 ± 70 days. It is worth to point out that data over North Europe are

severely affected by missing values during winter time (due to persistent cloud coverage and low solar angle), which likely affect the estimates of start/end dates and underestimate the length of the period between these two dates.

The most notable difference in the observed dynamics is that, while Central and North Europe fAPAR are relatively in-phase with the incoming solar radiation (with maximum values occurring during summer), the data over Mediterranean countries are off-phase (maximum values in early spring); the latter are mainly due to the severe water stress that occurs over these areas during summer. Overall, the observed dynamics are in agreement with the ground observed datasets (i.e., from flux towers) reported in [20] [21].

Finally, the plots in Figure 4 report three examples of fAPAR time series, as well as the transition points as detected by the applied methodology. The three sites were selected with the aim of illustrating the performance of the methodology over different conditions. These plots clearly highlight the good capability of the proposed procedure to identify the presence of single or multiple cycles, as well as of the piecewise logistic approach to capture the true dynamic of fAPAR. In particular, the plot in Figure 4c highlights the capability of the method to detect also the secondary transition points that occur between the two primary cycles, which can be used to further discriminate among different fAPAR time series behaviors.

IV. SUMMARY AND CONCLUSIONS

This paper evidences the flexibility of an approach based on piecewise logistic functions to automatically capture the dynamic of fAPAR over a large area, such as the European continent. The methodology allows identifying the main transition dates between increasing and decreasing periods in a consistent framework by exploiting the information content of the fAPAR dataset itself. The fitting of a continuous function for the computation of the transition dates, rather than the use of a discrete numerical detection, allows for a more coherent spatial definition of these dates.

The obtained results highlight a large variety of the vegetation dynamic within the studies domain, suggesting that the fAPAR anomalies occurring in the same decade over different areas may represent different effects on ecosystems due to the different phenological stages (e.g., green-up, senescence, etc.) at which those anomalies manifest. Additionally, the likely interannual variability of the detected transition dates should be analyzed in the current framework of climate change.

Improvements of the proposed modelling framework can be derive from quantitative comparisons of the retrieved key dates against ground observations; overall, these results can be considered a promising starting point for a more ecosystem-driven analysis of drought phenomena over Europe, which may be based on combining the information on the current phenological stage with the anomaly compared to the climatology.

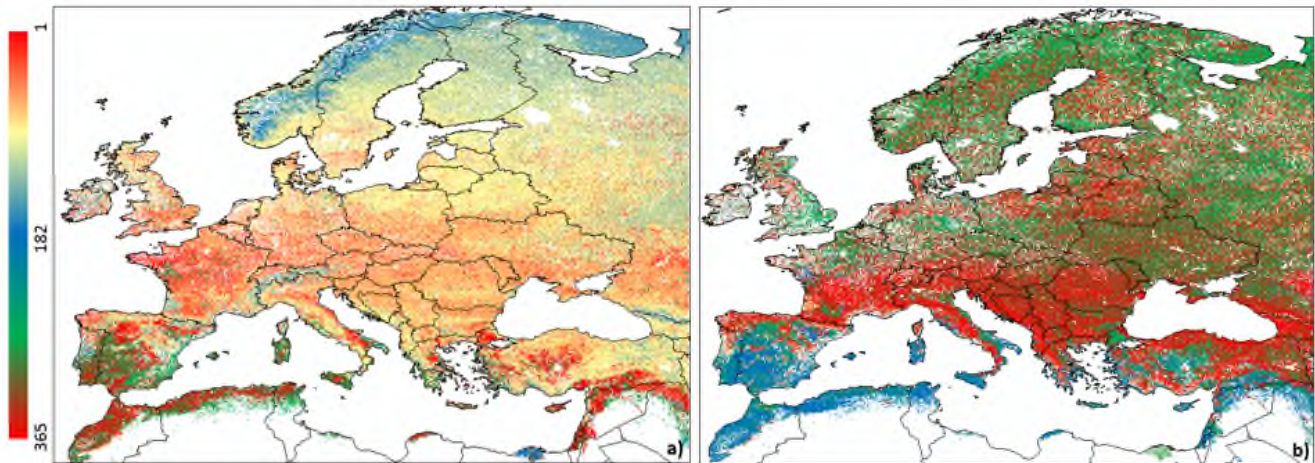


Figure 3. Spatial distribution of the two main transition dates (as Day Of the Year, DOY): (a) start of the fAPAR increasing period, (b) end of the fAPAR decreasing period.

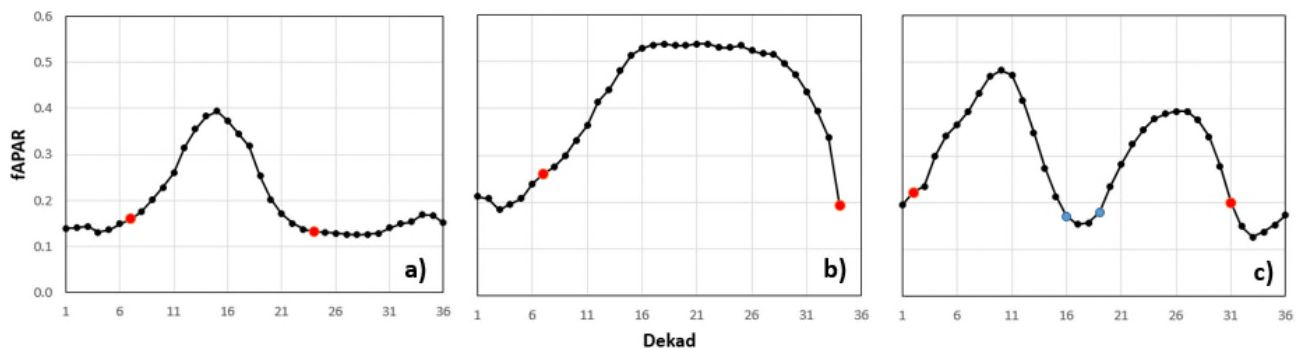


Figure 4. Example of fAPAR time series with main transition dates (red dots), as well as secondary ones (blue dots) in case of multiple peaks, for the sites: (a) South of Skopje (Macedonia), (b) North of Basel (Switzerland), and (c) Hatay region in Turkey.

ACKNOWLEDGMENT

The authors thank the NASA Land Process Distributed Active Archive Center (DAAC, <https://lpdaac.usgs.gov/>) for making the Terra MODIS satellite images freely available for download.

REFERENCES

[1] GCOS, "Summary report of the ninth session of the GCOS/GTOS terrestrial observation panel for climate," WMO/TD No.1371, Ispra (Italy), 28-29 March, 2007.

[2] N. Gobron et al., "The state vegetation in Europe following the 2003 drought," *Int. J. Remote Sens. Lett.*, vol. 26, 2005, pp. 2013-2020.

[3] S. Rossi and S. Niemeyer, "Drought monitoring with estimates of the fraction of absorbed photosynthetically-active radiation (fAPAR) derived from MERIS," in: *Remote Sensing of Drought: Innovative Monitoring Approaches*, B.D. Wardlow, M.C. Anderson and J.P. Verdin Eds., Boca Raton, FL, CRC Press, 2012.

[4] <http://edo.jrc.ec.europa.eu>. (Accessed on: May 24, 2016).

[5] G. Sepulcre-Canto, S. Horion, A. Singleton, H. Carrao, and J. Vogt, "Development of a combined drought indicator to detect agricultural drought in Europe," *Nat. Hazards Earth Syst. Sci.*, vol. 12, 2012, pp. 3519-3531.

[6] S. Rossi et al., "Potential of MERIS fAPAR for drought detection," in *Proceedings of the 2nd MERIS/(A)ATSR User Workshop*, ESA SP-666, H. Lacoste and L. Ouwehand Eds., Frascati, Italy, ESA Communication production Office, 2008, 6 pp.

[7] P.D. Jamieson, R.J. Martin, G.S. Francis, and D.R. Wilson, "Drought effects on biomass production and radiation-use efficiency in barley," *Field Crop. Res.*, vol. 43, n. 2-3, 1995, pp. 77-86.

[8] M. Linderman, Y. Zeng, and P. Rowhani, "Climate and land-use effects on interannual fAPAR variability from MODIS 250 m data," *Photogram. Eng. Remote Sens.*, vol. 76, n. 7, 2010, pp. 807-816.

[9] D. Lloyd, "A phenological classification of terrestrial vegetation cover using shortwave vegetation index imagery," *Int. J. Remote Sens.*, vol. 11, 1990, pp. 2269-2279.

[10] B.C. Reed et al., "Measuring phenological variability from satellite imagery," *J. Veg. Sci.*, vol. 7, 1994, pp. 703-714.

[11] E. Ivits et al., "Combining satellite derived phenology with climate data for climate change impact assessment," *Glob. Plan. Change*, vol. 88-89, 2012, pp. 85-97.

[12] M. Menenti, S. Azzali, W. Verhoef, and R. van Swol, "Mapping agroecological zones and time-lag in vegetation growth by means of Fourier-analysis of time-series of NDVI images," *Adv. Space Res.*, vol. 13, n. 5, 1993, pp. 233-237.

- [13] X. Zhang, et al., "Monitoring vegetation phenology using MODIS," *Remote Sens. Environ.*, vol. 84, 2002, pp. 471-475.
- [14] G.D. Badhwar, "Automatic corn-soybean classification using Landsat MSS data: II. Early season crop proportion estimation," *Remote Sens. Environ.*, vol. 14, 1984, pp. 31-37.
- [15] C. Atzberger, A. Klish, M. Mattiuzzi, and F. Vuolo, "Phenological metrics derived over the European continent from NDVI3g data and MODIS time series," *Remote Sens.*, vol. 6, n. 1, 2013, pp. 257-284.
- [16] R.B. Myneni, Y. Knyazikhin, J. Glassy, P. Votava, and N. Shabanov, "FPAR, LAI (ESDT: MOD15A2) 8-day Composite NASA MODIS Land Algorithm. User's Guide," 2003, 17 pp.
- [17] Y. Knyazikhin, J.V. Martonchik, R.B. Myneni, D.J. Diner, and S.W. Running, "Synergistic algorithm for estimating vegetation canopy leaf area index and fraction of absorbed photosynthetically active radiation from MODIS and MISR data," *J. Geophys. Res.*, vol. 103, 1998, pp. 32257-32274.
- [18] R.G. Brown and R.F. Meyer, "The fundamental theory of exponential smoothing," *Operat. Res.*, vol. 9, 1961, pp. 673-685.
- [19] D. Villegas, N. Aparicio, R. Blanco, and C. RoYo, "Biomass accumulation and main stem elongation of durum wheat grown under Mediterranean conditions," *Ann. Bot.*, vol. 88, 2001, pp. 617-627.
- [20] J.M. Paruelo, et al., "Temporal and spatial patterns of ecosystem functioning in protected arid areas in southeastern Spain," *Appl. Veg. Sci.*, vol. 8, 2005, pp. 93-102.
- [21] P. D'Odorico, et al., "Intercomparison of fraction of absorbed photosynthetically active radiation products derived from satellite data over Europe," *Remote Sens. Environ.*, vol. 142, 2014, pp. 141-154.